

# ornl

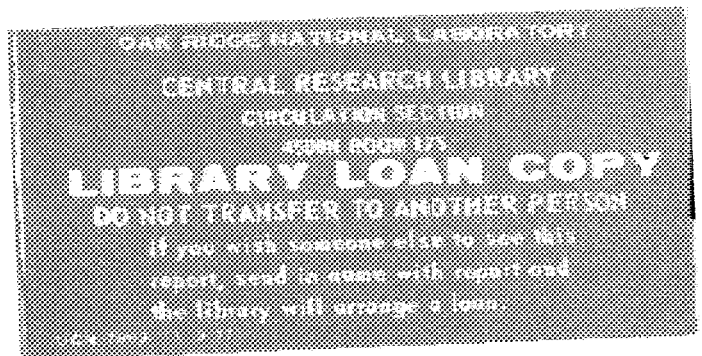
ORNL/TM-10996

**OAK RIDGE  
NATIONAL  
LABORATORY**

**MARTIN MARIETTA**

## **Calorimeter and Related Calculations for the Superconducting Super Collider**

T. A. Gabriel



OPERATED BY  
MARTIN MARIETTA ENERGY SYSTEMS, INC.  
FOR THE UNITED STATES  
DEPARTMENT OF ENERGY

Printed in the United States of America. Available from  
National Technical Information Service  
U.S. Department of Commerce  
5285 Port Royal Road, Springfield, Virginia 22161  
NTIS price codes—Printed Copy: A03; Microfiche A01

This report was prepared as an account of work sponsored by an agency of the United States Government. Neither the United States Government nor any agency thereof, nor any of their employees, makes any warranty, express or implied, or assumes any legal liability or responsibility for the accuracy, completeness, or usefulness of any information, apparatus, product, or process disclosed, or represents that its use would not infringe privately owned rights. Reference herein to any specific commercial product, process, or service by trade name, trademark, manufacturer, or otherwise, does not necessarily constitute or imply its endorsement, recommendation, or favoring by the United States Government or any agency thereof. The views and opinions of authors expressed herein do not necessarily state or reflect those of the United States Government or any agency thereof.

ORNL/TM-10996

Engineering Physics and Mathematics

**Calorimeter and Related Calculations  
for the Superconducting Super Collider\***

T. A. Gabriel

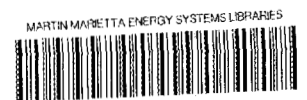
\*Submitted for journal publication.

Prepared for Office of High Energy & Nuclear Physics

DATE PUBLISHED — February 1989

**NOTICE:** This document contains information of a preliminary nature. It is subject to revision or correction and therefore does not represent a final report.

Prepared by the  
OAK RIDGE NATIONAL LABORATORY  
Oak Ridge, Tennessee 37831  
operated by  
MARTIN MARIETTA ENERGY SYSTEMS, INC.  
for the  
U.S. DEPARTMENT OF ENERGY  
under contract DE-AC05-84OR21400



3 4456 0289323 3



## CONTENTS

ABSTRACT . . . . .	vii
1. THE CALOR CODE PACKAGE . . . . .	1
2. COMPENSATED CALORIMETRY . . . . .	5
3. SILICON CALORIMETRY . . . . .	7
4. RADIATION DAMAGE STUDIES AT THE SSC . . . . .	13
REFERENCES . . . . .	18



## LIST OF FIGURES

<u>Figure</u>		<u>Page</u>
1	Flow diagram of the CALOR system . . . . .	2
2	Effective energy deposition vs. charged particle energy for several different types of particles. Similar curves are used for plastic scintillator . . . . .	4
3	Pulse height produced by a Si recoil atom relative to that of an electron of the same energy in Si as a function of Si recoil energy. The incident monoenergetic neutron energy necessary to produce the denoted recoil energy in a backscattering event is shown in parentheses. The solid line denotes predictions of Lindhard et al., as described in Ref. 17, the source of these data . . . . .	8
4	The calculation of the measured hadron energy distribution for 10 GeV $\pi^-$ incident on a uranium-silicon calorimeter with 5 mm thick uranium radiators and 400 $\mu\text{m}$ fully depleted detectors imbedded in 5mm thick G10 supports . . . . .	9
5	The calculated variation of $e/\pi$ and $\sigma/\sqrt{E}$ with the thickness of a G10 sheet placed between the 2mm uranium-silicon calorimeter and the silicon detectors. Without G10 a slight overcompensation condition exists, while as the thickness of G10 increases, the $e/\pi$ ratio passes through 1. These calculations were done for incident 10 GeV $\pi^-$ . . . . .	10
6	The calculated measured hadron energy distribution for 10 GeV $\pi^-$ incident on a uranium-silicon calorimeter with 2 mm thick uranium radiators and 400 $\mu\text{m}$ fully depleted detectors with a 1.6 mm G10 layer behind the uranium and in front of the silicon layers . . . . .	12
7	Calculated longitudinal distributions of neutron flux ( $40 \text{ keV} < E < 20 \text{ MeV}$ ) in the Tevatron tunnel for 875 GeV incident proton energy (histograms), and measured distribution from Ref. 21. The calculated initial collision point of the protons is at 0. The experimental collision points occur approximately uniformly over $\pm 8 \text{ m}$ around 0 . . . . .	14
8	Calculated energy spectrum of the total neutron flux near the maximum of the longitudinal distribution in an 875 GeV simulation (histogram), and the result of processing these data through the Bonner sphere spectrometer and unfolding program LOUHI (smooth curve) . . . . .	16

<u>Figure</u>	<u>Page</u>
9	
Preliminary neutron spectra observed near the tunnel wall near the Tevatron ring in 1987 [21]. The solid curve is for production from N <sub>2</sub> in the warm section, and the dashed curve for background of unknown origin (at extrapolated zero pressure). Normalization of the solid curve is absolute for $z = 10$ m pending pressure gauge calibration and other corrections, while that of the dashed curve is of necessity arbitrary. The Bonner sphere spectrometer data were unfolded using program LOUHI . . . . .	
	17

## ABSTRACT

There are four topics to be covered in this paper. The first topic deals with the programs, the models, and the cross sections in the CALOR code package. Secondly, a discussion on compensating calorimetry as it applies to Fe/Si and U/Si calorimetry will be given. Thirdly, calculated results obtained on U/Si calorimeters using the CALOR system will be presented and discussed. Finally, the calculations that the Oak Ridge National Laboratory are carrying out dealing with radiation damage at the proposed Superconducting Super Collider (SSC) are described.



# 1. THE CALOR CODE PACKAGE

The calculations that will be presented here were performed with the CALOR computer system following approximately the procedures used in previous calculations.<sup>1,2,3</sup> A flow diagram of the codes in CALOR is given in Fig. 1. The three-dimensional, multimedia, high-energy nucleon-meson transport code, HETC,<sup>4</sup> was used, with modifications, to obtain a detailed description of the nucleon-meson cascade produced in the devices considered in this paper. This Monte Carlo code takes into account the slowing down of charged particles via the continuous slowing-down approximation, the decay of charged pions and muons, inelastic nucleon-nucleus and charged-pion-nucleus (excluding hydrogen) collisions through the use of the intermediate-energy intranuclear-cascade-evaporation (MECC) model ( $E < 3$  GeV) and scaling model ( $E > 3$  GeV), and inelastic nucleon-hydrogen and charged-pion-hydrogen collisions via the isobar model ( $E < 3$  GeV) and phenomenological fits to experimental data ( $E > 3$  GeV). Also accounted for are elastic neutron-nucleus ( $E < 100$  MeV) collisions, and elastic nucleon and charged-pion collisions with hydrogen.

The intranuclear-cascade-evaporation model as implemented by Bertini is the heart of the HETC code.<sup>5</sup> This model has been used for a variety of calculations and has been shown to agree quite well with many experimental results. The underlying assumption of this model is that particle-nucleus interactions can be treated as a series of two-body collisions within the nucleus and that the location of the collision and resulting particles from the collisions are governed by experimental and/or theoretical particle-particle total and differential cross section data. The types of particle collisions included in the calculations are elastic, nonelastic and charge exchange. This model incorporates the diffuseness of the nuclear edge, the Fermi motion of the bound nucleons, the exclusion-principle, and a local potential for nucleons and pions. The density of the neutrons and protons within the nucleus (which is used with the total cross sections to determine interaction locations) are determined from the experimental data of Hofstadter.<sup>5</sup> Nuclear potentials are determined from these density profiles by using a zero-temperature Fermi distribution. The total well depth is then defined as the Fermi energy plus 7 MeV.

Following the cascade part of the interaction, excitation energy remains in the nucleus. This energy is treated by using an evaporation model which allows for the emission of protons, neutrons, d,  $^3\text{He}$ ,  $\alpha$  and t. Fission, induced by high-energy particles, is accounted for during this phase of the calculation by allowing it to compete with evaporation. Whether or not a detailed fission model is included has very little effect on the total number of secondary neutrons produced.

The source for the electromagnetic cascade calculation is provided by HETC and consists of photons from neutral pion decay, electrons and positrons from muon decay (although this is usually not of interest in calorimeter calculations because of the long muon lifetime), deexcitation gamma rays from nonelastic nuclear collisions and fission gamma rays. Since the discrete decay energies of the deexcitation gammas are not provided by HETC and only the total energy is known, individual gamma energies are obtained by uniformly sampling from the available energy until it is completely depleted. The transport of the electrons, positrons, and gammas from the above sources is carried out using the EGS system.<sup>6</sup>

2 *The CALOR Code Package*

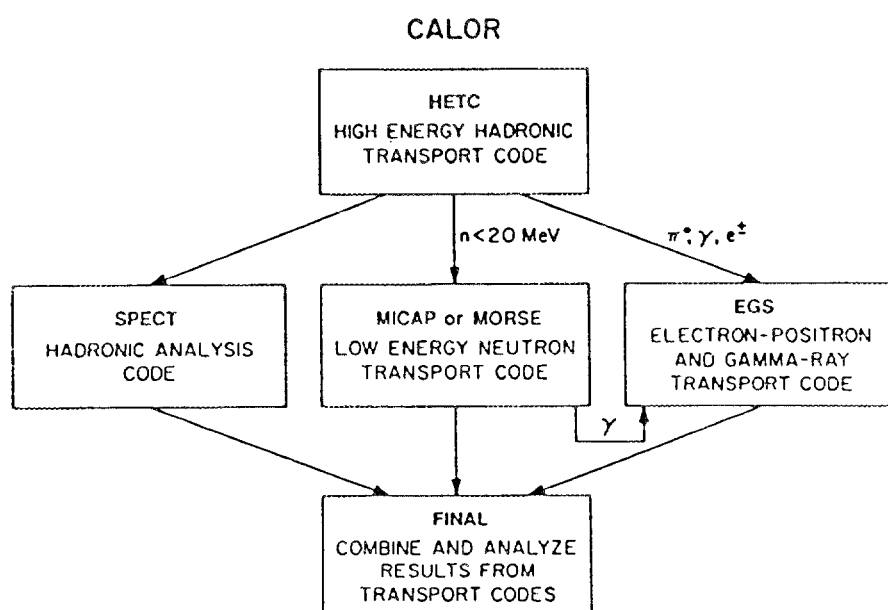


Figure 1. Flow diagram of the CALOR system.

Neutrons which are produced with energies below 20 MeV are transported using the MORSE<sup>7,8</sup> Monte Carlo transport code. The neutron cross sections used by MORSE were obtained from ENDF/B-IV. Gamma rays (including those from capture, fission, etc.) produced during this phase of the calculations are stored for transport by the EGS code. The MORSE code was developed for reactor application and can treat fissioning systems in detail. This ability is very important since a majority of the fissions in uranium calorimeters results from neutrons with energies less than 20 MeV. Time-dependence is included in MORSE, but since neither HETC nor EGS has a timing scheme incorporated, it has been assumed that no time passes for this phase of the particle cascade. Therefore, all neutrons below 20 MeV are produced at  $t = 0$ . General time cuts used in the MORSE code are 50 ns for scintillator and 100 ns for TMS or liquid argon.

The nonlinearity of the light pulse,  $L$ , in scintillator due to saturation effects is taken into account by the use of Birks' law.<sup>9</sup>

$$\frac{dL}{dx} \propto \frac{dE/dx}{1 + k_B dE/dx},$$

where  $k_B$  is the saturation constant. For plastic scintillator  $k_B = 0.01 \text{ g cm}^{-2} \text{ MeV}^{-1}$ . A similar law is assumed to apply to the charge collected in ionization detectors. This takes into account the loss of signal resulting from recombination effects in the ionization column.<sup>10</sup> For electrons at all energies, it is assumed that  $k_B = 0$ . An example of these data are given in Fig. 2.

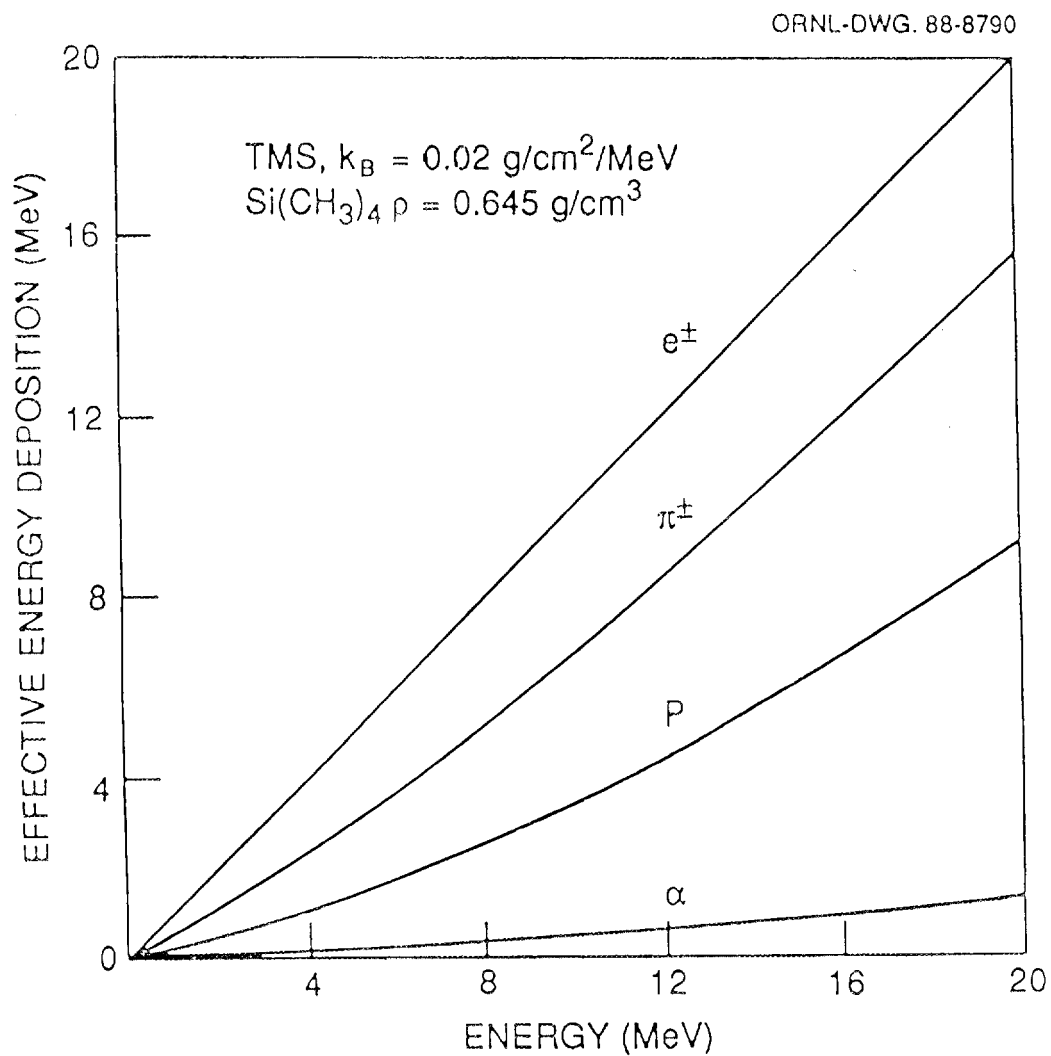


Figure 2. Effective energy deposition vs. charged particle energy for several different types of particles. Similar curves are used for plastic scintillator.

## 2. COMPENSATED CALORIMETRY

The first requirements of a hadron calorimeter design are to make it large enough to contain most of the hadronic shower and to have enough samples that sampling fluctuations are small. Assuming these, the two most important parameters of a hadron calorimeter, the energy resolution and the ratio of the most probable signal from an electron to that from a hadron of the same energy ( $e/h$ ) will be dominated by fluctuations in the hadron shower and losses due to nuclear binding energy. In calorimeter design it is usually assumed that the active medium samples the shower in the passive medium in detail, and that for both the incident radiation and the secondary radiation, the signal output from the active medium is the same fixed fraction of the energy deposited in the passive medium. While this is approximately true for electromagnetic calorimeters, it is far from the truth for hadron calorimeters. In practice, however, the active and passive media exhibit different characteristics when exposed to similar types of radiation. The active media often do not give similar response for the same energy deposition by different particles and the energy sampling is not equal in the active region for electrons, low-energy neutrons, and gamma rays. Calorimeters which utilize iron or low atomic weight (A) materials as the passive media exhibit an almost equal distribution of the cascade energy into protons, neutrons, charged pions and neutral pions for intermediate incident energy (1-20 GeV) hadrons. On the contrary, if Pb, Ta, or U is used as the passive material, the energy distribution among produced particles is shifted toward additional neutron production through spallation and fission. There are more secondary particles and the energy spectra of all of them are shifted toward lower energies. In calorimeters utilizing low A materials, the majority of the signal is from charged particles which are produced in the passive material and which pass through the active region. In calorimeters utilizing high A material, the signal from charged particles produced in the passive material is reduced relative to the energy deposition due to the neutral particles, in particular, low energy cascade neutrons of energy 1-20 MeV. To fully utilize this sizable fraction of energy left in the cascade due to these neutrons of energy less than 20 MeV, the detection medium itself must be sensitive through internal collisions with these particles. It is also possible to deliberately enhance the signal due to these low energy neutrons, relative to the signal from other particles by using an active medium which detects these neutrons with greater efficiency than the passive medium.

One way of enhancing this sensitivity to low energy neutrons is by using a hydrogenous active medium.<sup>11,12,13</sup> Hydrogen has a large cross section for neutron scattering, on the order of several  $\times 10^{-24}$  cm<sup>2</sup> for neutrons of energy of a few MeV. Hydrogen also allows for the largest energy transfer considering elastic scattering.<sup>11,12,13</sup> Proton production via nonelastic neutron collision with other nuclei in the active media will only consume binding energy and will not help substantially with the signal. With equal sensitivity of the active media to gamma rays, electrons, and neutrons, it can be shown that the choice of a hydrogenous active medium and a passive medium with high atomic number can overcompensate for the loss of hadron pulse height due to nuclear binding energy and lead to an  $e/h$  ratio less than unity. However, on the other hand, low energy recoil protons of a given energy produce in many detectors, a smaller signal than electrons or gamma

## 6 *Compensated Calorimetry*

rays of the same energy thereby reducing their effectiveness. (This is illustrated in Fig. 2.)

The use of uranium, as first suggested by Fabjan and Willis<sup>14</sup> offers a way to compensate and improve the resolution on an event-by-event basis for hadronic shower fluctuations and losses due to nuclear binding energy. The understanding of this compensation and improved resolution was initially not correctly understood.<sup>15,11,12,13</sup> These improvements can be understood from an examination of the hadronic cascade. If the particle cascade is strongly electromagnetic in character, that is, there is extensive production of neutral pions which decay into photons, the uranium will tend to suppress the electromagnetic part of the cascade due to sampling inefficiencies, that is, a larger fraction of the energy will be deposited in the U than would be expected by a simple analysis. However, if the cascade is strongly hadronic, there will be an amplification of the low energy neutrons, and to a lesser extent, gamma ray energy available due to hadronically produced cascade neutrons and fission neutrons, and neutron-induced fission, capture, and inelastic collisions leading to the emission of fission and capture gamma rays. Sampling inefficiencies are not as large for pure hadronic cascades, therefore the signal remains less affected. The combination of electromagnetic suppression and little hadronic suppression improves the resolution by narrowing the pulse height. However, if the active medium is not very sensitive to low energy neutrons only sampling inefficiencies will contribute to improvements in compensation; i.e., improvements in the  $e/h$  ratio. If liquid argon is chosen as the active medium, signals from the low energy neutron collisions with the argon atoms will be greatly suppressed due to saturation effects and small energy transfers.<sup>11,12,13</sup> If plastic, TMS, or TMP is chosen, the hydrogen will enable the low energy neutrons to produce proton recoils. However, saturation effects due to the inefficient light or charge production mechanism for low energy protons can limit their effectiveness. The liquid argon should be somewhat better for the detection of the low energy gamma rays, due to its large  $Z$  nucleus.<sup>12,13</sup>

### 3. SILICON CALORIMETRY

The understanding that now exists concerning compensating calorimeters can be applied to the silicon detector calorimeters.<sup>16</sup> The fundamental question that needs to be addressed is what the  $e/h$  ratio for these silicon based calorimeters will be. One property of silicon that plays an important role in this study is the extreme linearity of silicon up to very large stopping power. That is, silicon exhibits very little saturation. It has been demonstrated that saturation prevents full compensation in currently designed uranium-liquid argon calorimeters, so this could be a very important factor in silicon calorimeters. Naively, it is expected that very good results can be obtained for silicon calorimeters.

The linearity of response of silicon to large energy deposition densities is summarized in Fig. 3. Figure 3 shows the relative response of a recoil ion of maximal energy in neutron scattering.<sup>17</sup> It is evident that even for silicon ions as low as 100 keV, nearly one-half of the deposited energy is detected as observable output signal. Given these evidences of very limited saturation in silicon detectors, a very good response to some components of the low energy development of hadronic showers can be expected.

The potential for compensation with silicon certainly seems better than for liquid argon due to energy transfers by low energy neutrons and to saturation consideration. Figure 4 shows the calculated response distribution for 10 GeV pions incident on a silicon calorimeter with 5 millimeter thick uranium radiators and 400  $\mu\text{m}$  fully depleted silicon detectors sandwiched between two layers of 5 millimeter thick G10. Therefore, the total layer thickness is 15.4 millimeters and the depth of the stack extends for 150 readout and radiator layers. The transverse dimensions of the stack have been taken to be  $100 \times 100 \text{ cm}^2$ . The charge collection is cut off after 50 nanoseconds. The resulting energy resolution ( $\sigma/E$ ) is 21.5% and the  $e/h$  ratio is 1.07, close to compensation.<sup>18</sup> In fact, the two layers of G10 in this stack are increasing the value of  $e/h$  as the neutron energy from the uranium is being deposited in the G10 through the large energy transfers via hydrogen. Additionally, significant transfers occur to the carbon and oxygen in the G10.

Figure 5 presents a series of calculated results for calorimeters constructed with 2 mm uranium radiators, followed by a layer of G10 of varying thickness and a 400  $\mu\text{m}$  fully depleted silicon detector. As before,  $kB = 0$ , the time cut is 50 nanoseconds, and the transverse size is taken to be  $100 \times 100 \text{ cm}^2$ . The stacks contain 330 layers of uranium, G10, and silicon. It can be seen that with no G10 the condition of overcompensation is obtained due to the sensitivity of the silicon detectors to very low energy particles. As the G10 is added, the  $e/h$  ratio increases due to the removal of neutron energy by the G10, meaning less energy is available to be deposited in the silicon. Naively, one might expect that the neutrons interacting in the G10 would contribute to the response of the silicon by knocking protons into the detectors. It has been proposed that coupling a hydrogenous material to liquid argon, for example, would be a possible method for restoring its potential for compensation. However, the efficiency and range of the protons produced in the G10 is not large enough to have much of an effect on the total response of a detector of 400  $\mu\text{m}$  thickness.<sup>19</sup> It can also be seen in Fig. 5 that the energy resolution reaches a minimum at approximately the point where the  $e/h$  ratio passes through one, as

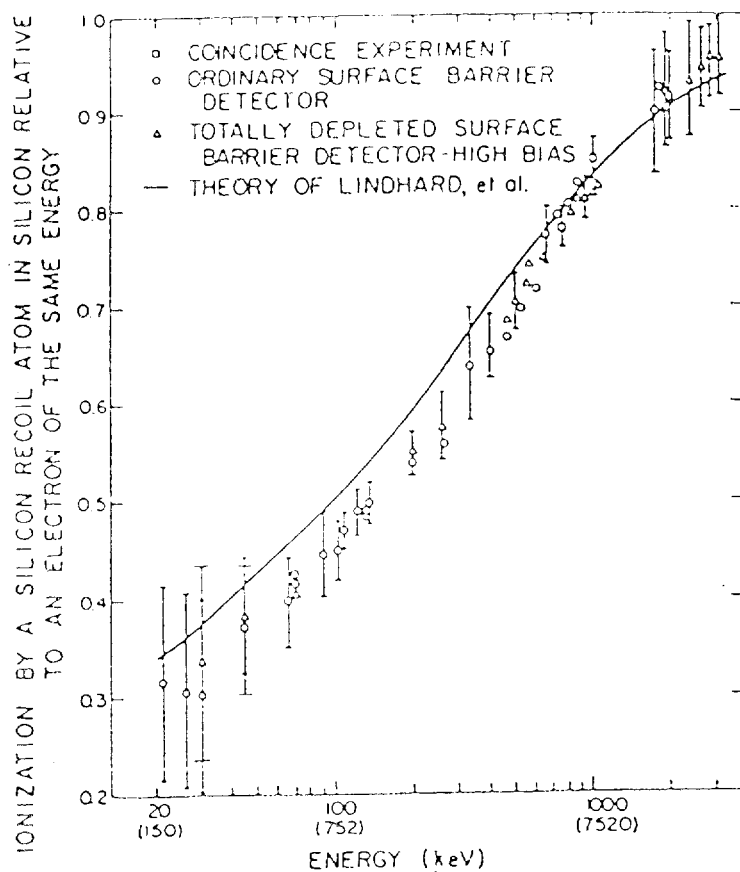


Figure 3. Pulse height produced by a Si recoil atom relative to that of an electron of the same energy in Si as a function of Si recoil energy. The incident monoenergetic neutron energy necessary to produce the denoted recoil energy in a backscattering event is shown in parentheses. The solid line denotes predictions of Lindhard et al., as described in Ref. 17, the source of these data.

## Uranium/silicon (5mm/5mm/0.4mm)

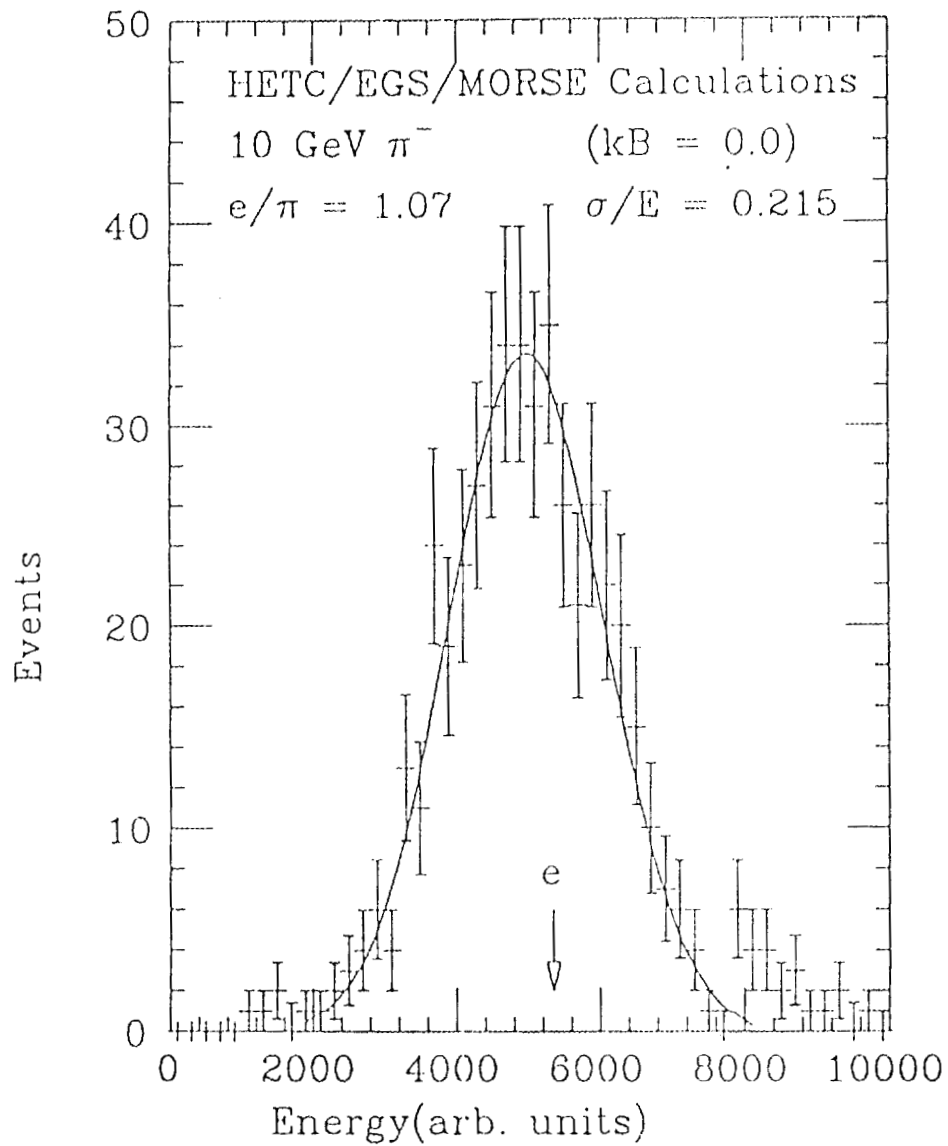


Figure 4. The calculation of the measured hadron energy distribution for 10 GeV  $\pi^-$  incident on a uranium-silicon calorimeter with 5 mm thick uranium radiators and 400  $\mu\text{m}$  fully depleted detectors imbedded in 5mm thick G10 supports.

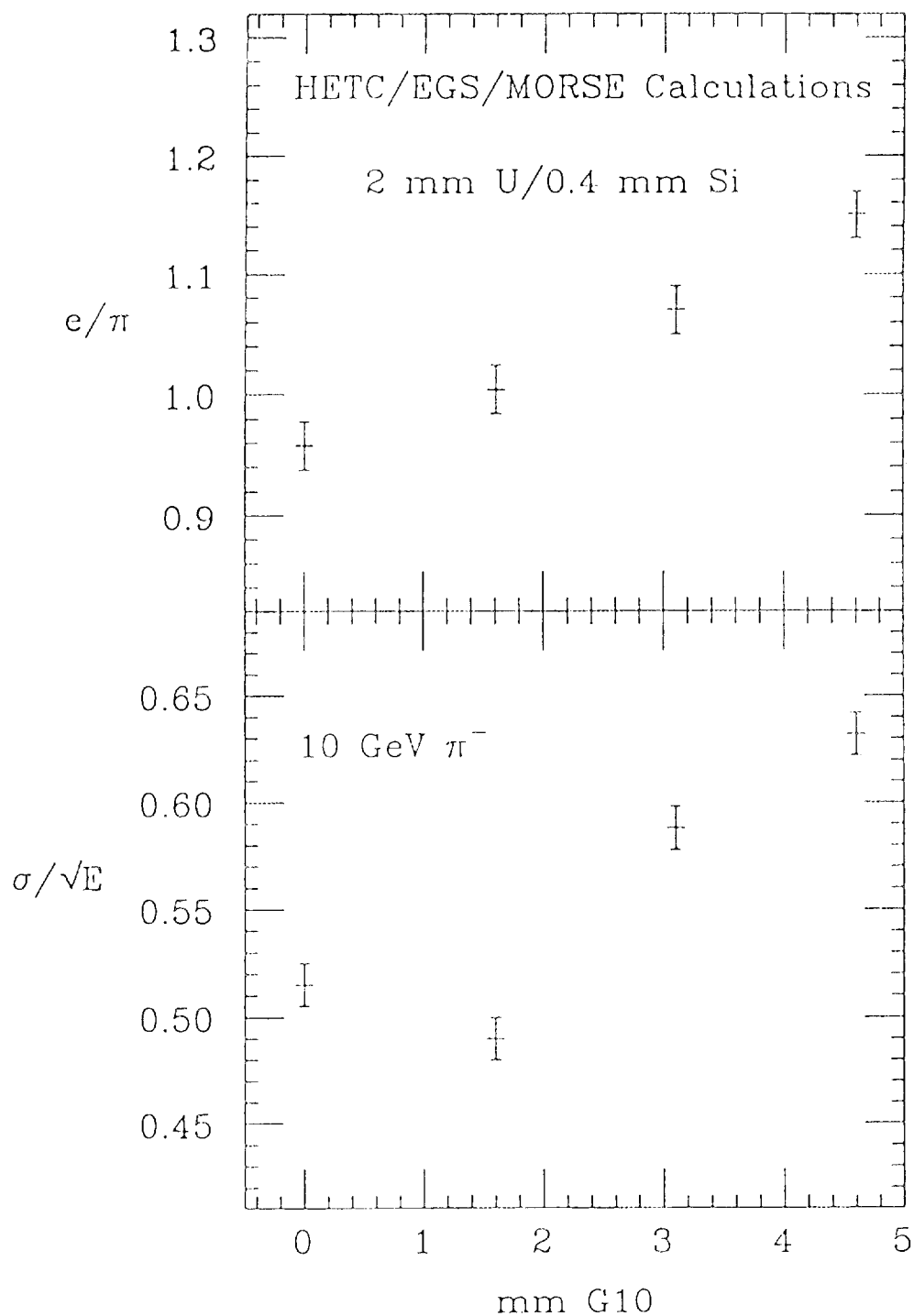


Figure 5. The calculated variation of  $e/\pi$  and  $\sigma/\sqrt{E}$  with the thickness of a G10 sheet placed between the 2mm uranium-silicon calorimeter and the silicon detectors. Without G10 a slight overcompensation condition exists, while as the thickness of G10 increases, the  $e/\pi$  ratio passes through 1. These calculations were done for incident 10 GeV  $\pi^-$ .

would be expected for a compensating calorimeter. The value of this resolution is not as small as the values achieved in scintillator because of the larger sampling fluctuations involved here. Figure 6 shows the distribution of measured energies for the 10 GeV  $\pi^-$  incident upon the optimal device shown in Fig. 5, that with 1.6 millimeters of G10. The distribution shows a well-behaved, nearly Gaussian shape.

Uranium/silicon (2mm/1.6mm/0.4mm)

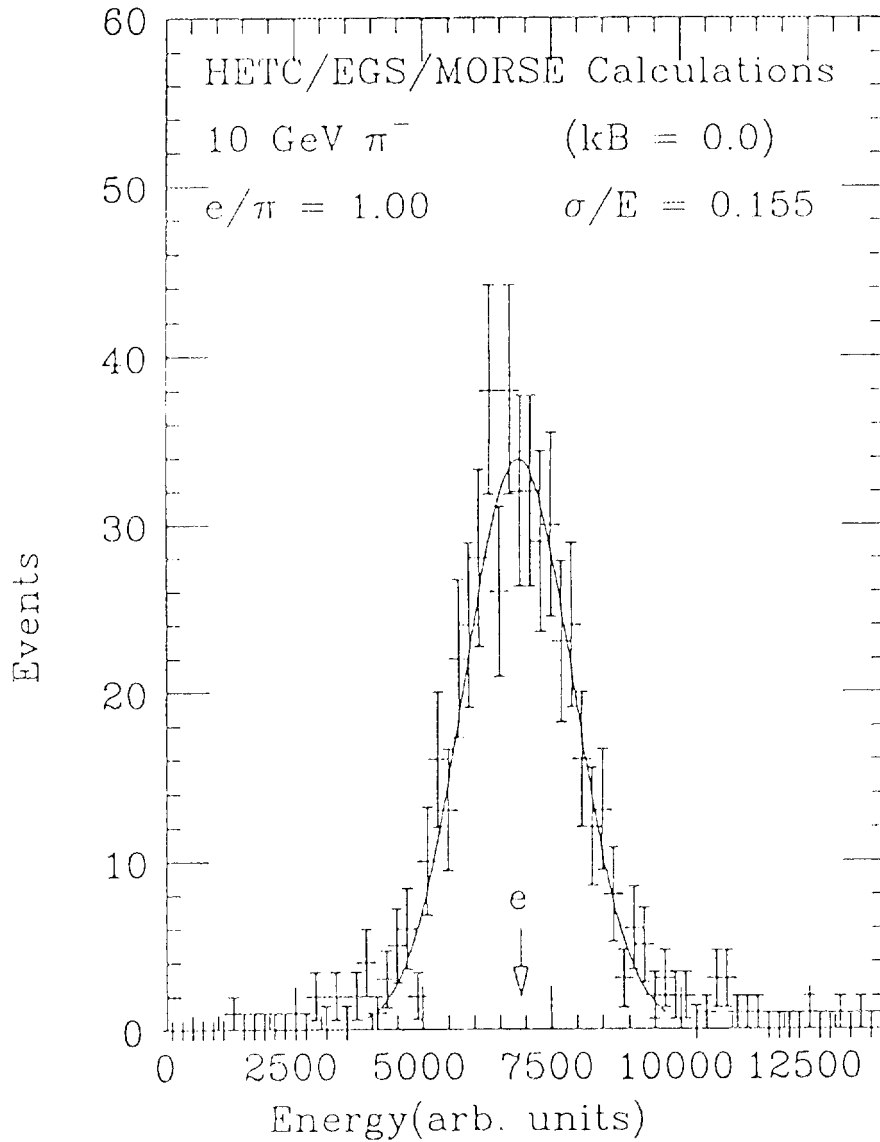


Figure 6. The calculated measured hadron energy distribution for 10 GeV  $\pi^-$  incident on a uranium-silicon calorimeter with 2 mm thick uranium radiators and 400  $\mu\text{m}$  fully depleted detectors with a 1.6 mm G10 layer behind the uranium and in front of the silicon layers.

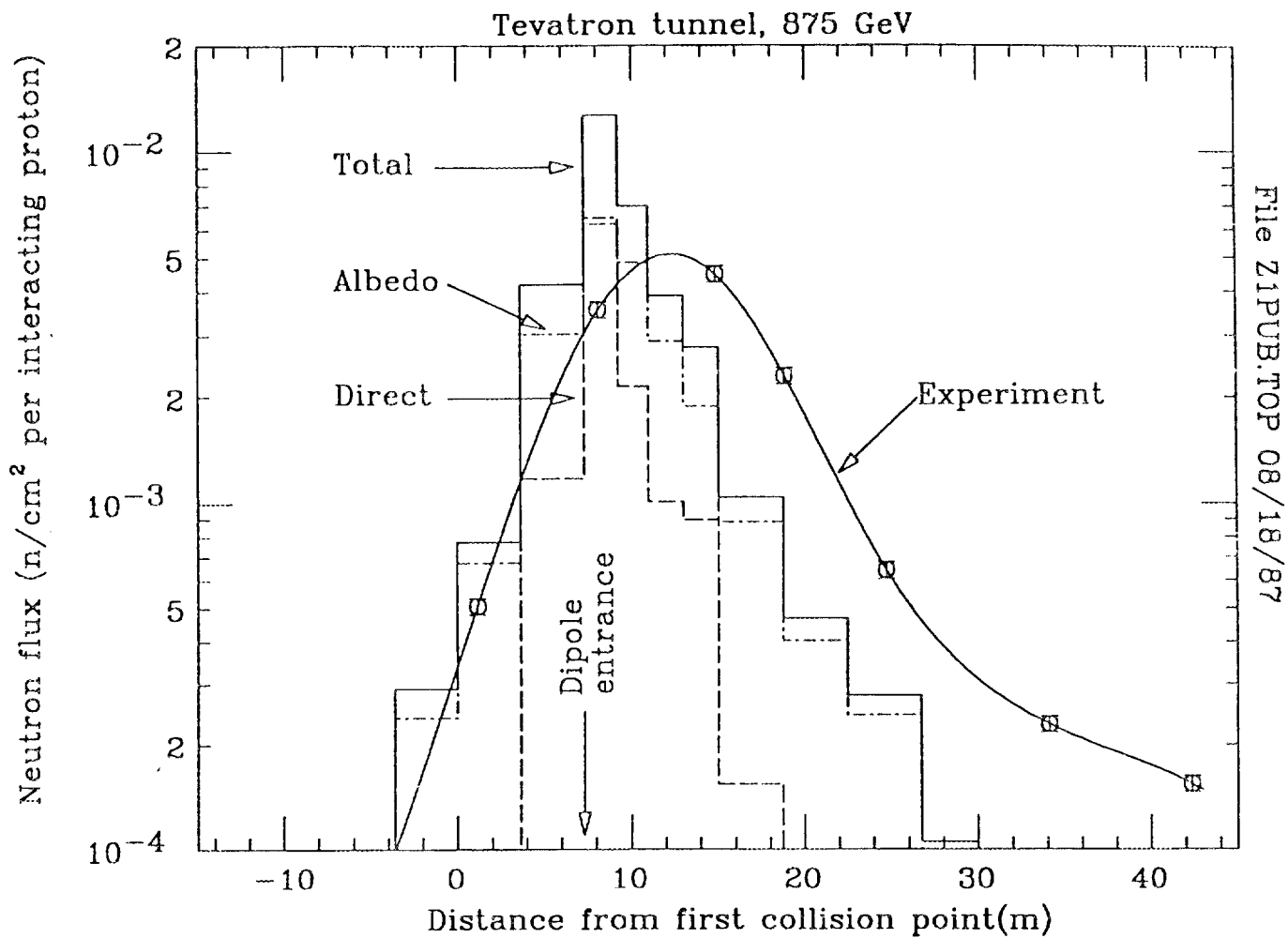
## 4. RADIATION DAMAGE STUDIES AT THE SSC

In the fall of 1985, a FNAL/LBL group measured neutron spectra in the TEVATRON tunnel.<sup>20</sup> During the machine cycle just ended (early 1987), these experiments were refined and extended.<sup>21</sup> Absolute magnitude and longitudinal distributions of the neutron flux were measured down the tunnel from a warm section in the beam pipe. A controlled N<sub>2</sub> gas leak was introduced near the center of the warm section, so that by measuring counting rates as a function of gas pressure, beam-gas rates could be separated from background rates. To help support this experimental effort, detailed simulations of particle cascades in the Fermilab tunnel initiated by hadron-nucleus collision ( $E_p = 875$  GeV) in the center of the warm section were carried out. The version of the HETC code used to carry out these hadron calculations has been modified to include a better hadron-nuclear collision model above 5 GeV (see Ref. 23). Cross section data for MORSE which carries out the transport of the neutrons with energies less than 20 MeV were obtained from the VITAMIN-E data library<sup>22</sup> and contain 53 neutron energy groups.

The study was motivated by concern about radiation damage to silicon semiconductors in the SSC tunnel. About 400 racks of control circuitry are located at 20 m intervals around the ring, and, in addition, a variety of temperature sensors, beam pickups, and perhaps quench protection diodes are mounted on or in each of the 10,000 magnets. If the results calculated at  $\approx 1$  TeV agree with experimental data, then confidence can be had when the calculations are carried out at 20 TeV, the SSC energy.

The longitudinal ( $z$ ) distribution (in the TEVATRON tunnel) of the total neutron flux above 40 keV and less than 20 MeV is shown in Fig. 7 for 875 GeV protons. Collisions at  $z = 0$  produce debris peaked in the forward direction, most of which enters the dipole aperture at 7.3 m. Charged particles are bent by the magnetic field (the effect of which has been included in the calculations) into the dipole yoke fairly quickly, where they initiate further cascades. Neutrals eventually hit the walls, at distances dependent upon their angles and the curve of the vacuum chamber.

The 875 GeV distribution shown in Fig. 7 peaks at about 8 m (about a meter past the entrance of the first dipole), then drops nearly exponentially. As expected, the albedo component, which is production by backscattering collisions in the tunnel wall, has a somewhat broader distribution than the direct component which comes directly from the primary collisions and secondary collisions in the magnet. Also shown in this figure by the solid curve is the preliminary experimental distribution. It is considerable broader, and peaks at larger  $z$ . The difference is due to the fact that the experimental source is distributed over nearly 16 meters in the warm straight section, whereas the initial proton collisions occur at  $z = 0$ . The areas under the  $z$ -distributions agree to within 9%.



File Z1PUB.TOP 08/18/87

Figure 7. Calculated longitudinal distributions of neutron flux ( $40 \text{ keV} < E < 20 \text{ MeV}$ ) in the Tevatron tunnel for 875 GeV incident proton energy (histograms), and measured distribution from Ref. 21. The calculated initial collision point of the protons is at 0. The experimental collision points occur approximately uniformly over  $\pm 8 \text{ m}$  around 0.

The energy spectrum obtained for 875 GeV incident protons is shown by the histogram in Fig. 8. Before comparing with experimental results, it should be noted that the simulations provide a *source* spectrum, while the experiment provides the actual source spectrum *as processed through the Bonner sphere spectrometer and unfolding routine* (see Fig. 9). For comparison purposes, the calculated spectrum must be folded with the response of the Bonner sphere, and then unfolded to obtain the final spectrum. The result of this procedure is shown by the dashed curve in Fig. 8. It is typical for such a procedure to broaden a sharp input spectrum, and the slight degradation of the energy at maximum is evidently a consequence of the skewing of the peak toward lower energies. The output curve has been normalized to the same area above 40 keV.<sup>23</sup>

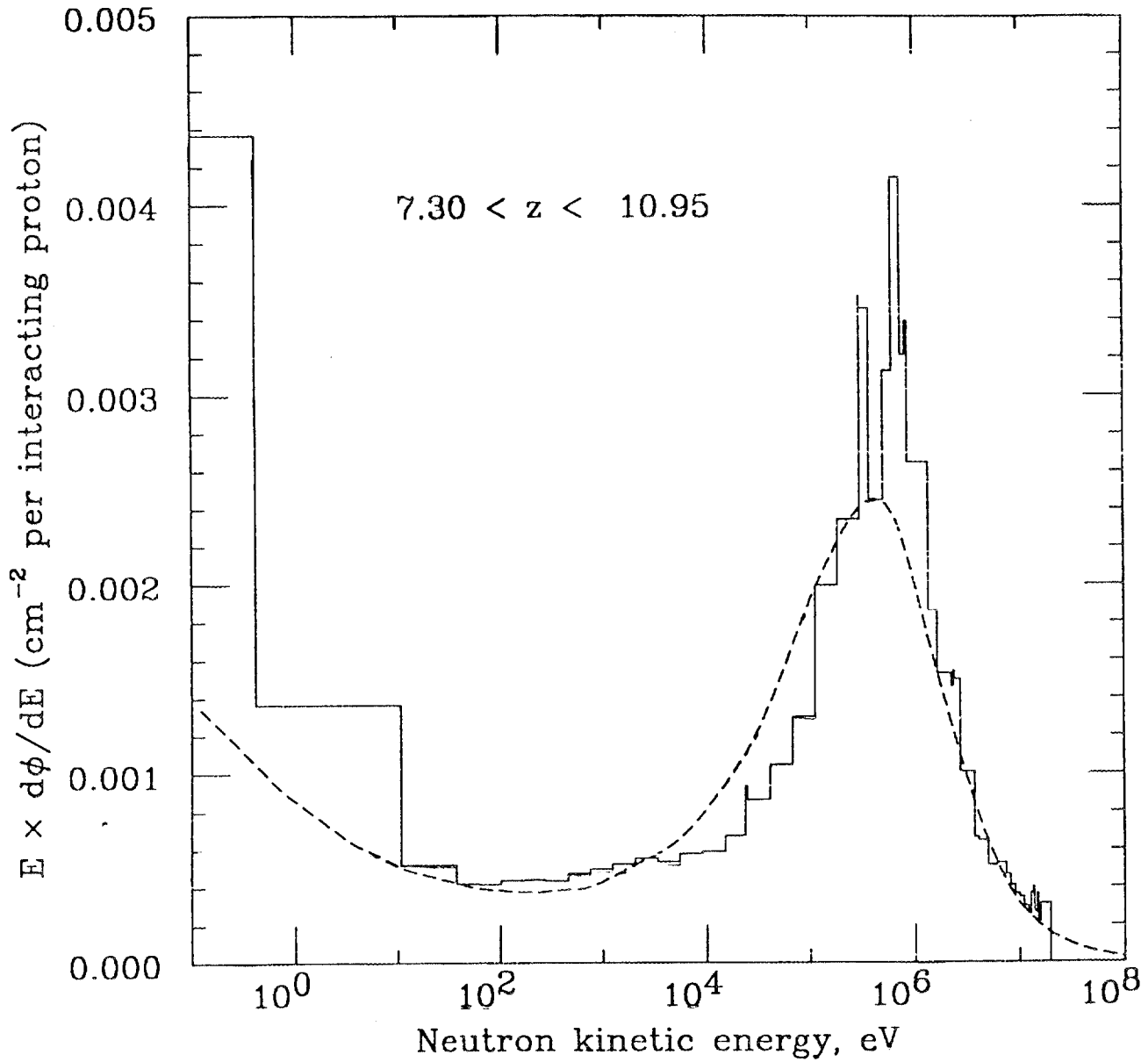


Figure 8. Calculated energy spectrum of the total neutron flux near the maximum of the longitudinal distribution in an 875 GeV simulation (histogram), and the result of processing these data through the Bonner sphere spectrometer and unfolding program LOUHI (smooth curve).

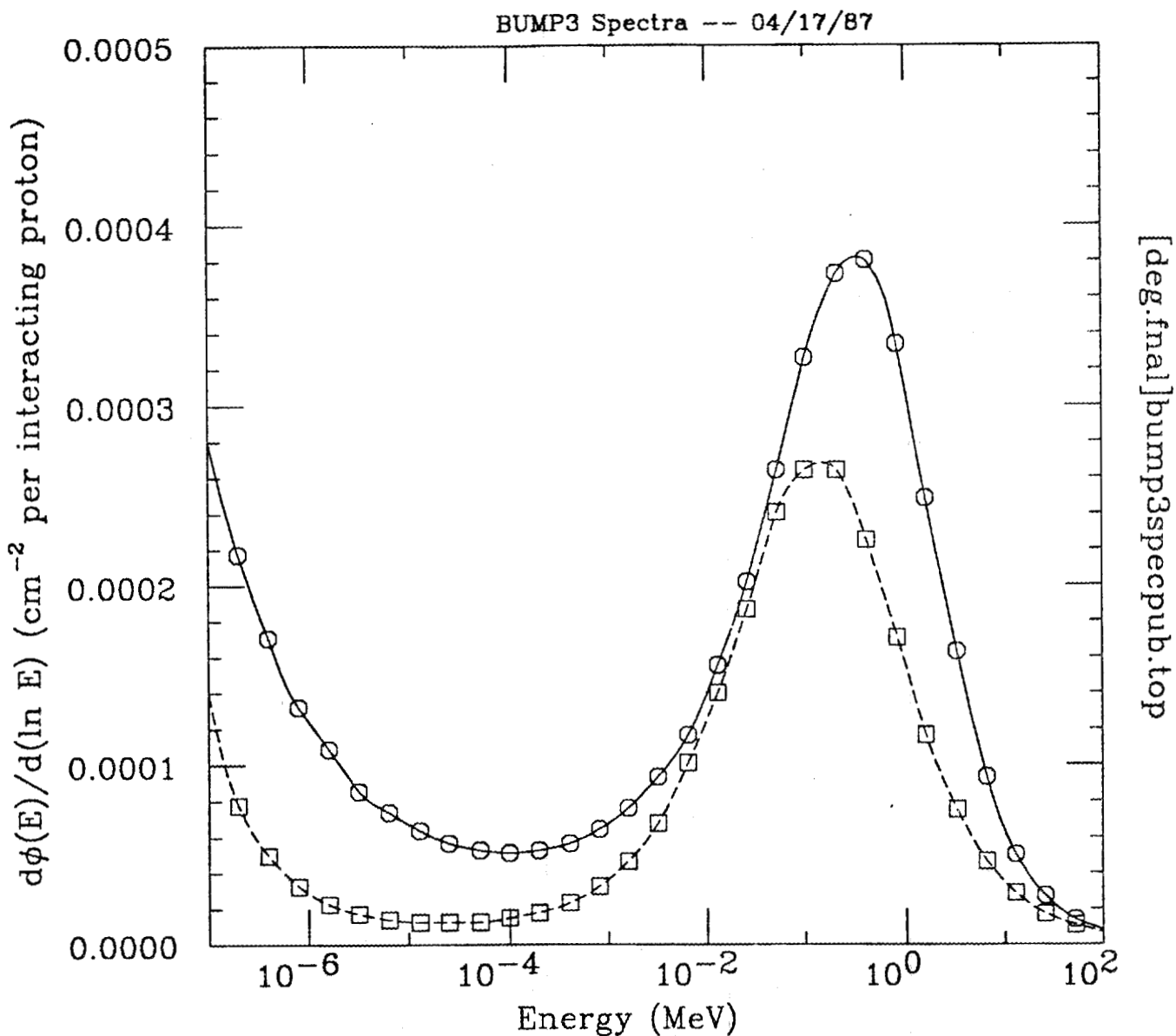


Figure 9. Preliminary neutron spectra observed near the tunnel wall near the Tevatron ring in 1987 [21]. The solid curve is for production from  $N_2$  in the warm section, and the dashed curve for background of unknown origin (at extrapolated zero pressure). Normalization of the solid curve is absolute for  $z = 10$  m pending pressure gauge calibration and other corrections, while that of the dashed curve is of necessity arbitrary. The Bonner sphere spectrometer data were unfolded using program LOUHI.

## REFERENCES

1. J. Brau and T. A. Gabriel, *Nucl. Instrum. & Methods* **238**, 489 (1985). T. A. Gabriel et al., *IEEE Trans. Nucl. Sci.* **NS-32**, 1 (1985).
2. T. A. Gabriel and W. Schmidt, *Nucl. Instrum. & Methods* **134**, 271 (1976).
3. T. A. Gabriel, *Nucl. Instrum. & Methods* **150**, 146 (1978).
4. T. A. Gabriel, "The High Energy Transport Code HETC," Oak Ridge National Laboratory, ORNL/TM-9727 (1985).
5. H. W. Bertini, *Phys. Rev.* **188**, 1711 (1969).
6. R. L. Ford and W. R. Nelson, Stanford Linear Accelerator Center, SLAC-0210 (1978).
7. M. B. Emmett, Oak Ridge National Laboratory, ORNL/TM-4972 (1975).
8. N. M. Greene et al., Oak Ridge National Laboratory, ORNL/TM-3706 (1973).
9. J. B. Birks, *Proc. Phys. Soc.* **A64**, 874 (1951).
10. A. Babaev et al., *Nucl. Instrum. & Methods* **160**, 427 (1979).
11. T. A. Gabriel et al., *IEEE Trans. Nucl. Sci.* **NS-32**, 1 (1985).
12. J. E. Brau and T. A. Gabriel, SLD - New Detector Note No. 119 (May 22, 1984).
13. See first listed reference under Ref. 1.
14. C. W. Fabjan et al., *Nucl. Instrum. & Methods* **141**, 61 (1977).
15. M. G. Albrow et al., *Nucl. Instrum. & Methods* **A265**, 303 (1988).
16. In collaboration with Dr. J. Brau, University of Tennessee, Knoxville, TN.
17. A. R. Sattler *Phys. Rev.* **138**, A1815 (1965).
18. It is emphasized that the  $e/h$  ratio was calculated assuming no saturation in the silicon.
19. T. A. Gabriel, J. O. Johnson, and J. E. Brau, "MICAP: A Program for Low Energy Neutron, Ion, and Gamma-Ray Transport and One of Its Applications in Calorimeter Design: Hydrogen Knock-in as a Method for Achieving Compensation," *Proceedings of the Workshop on Detector Simulation for the SSC*, Argonne National Laboratory, August 1987.
20. J. B. McCaslin et al., SSC Central Design Group Report No. SSC-58 (1986).
21. J. D. Cossairt et al., SSC Central Design Group Report, in preparation (1987).
22. R. W. Roussin et al., Radiation Shielding Information Center, Engineering Physics and Mathematics Division, Oak Ridge National Laboratory, DLC-113/VITAMIN-E.
23. T. A. Gabriel et al., "Preliminary Simulations of the Neutron Flux Levels in the Fermilab Tunnel and Proposed SSC Tunnel," SSC Central Design Group Report No. SSC-110.

## INTERNAL DISTRIBUTION

- |                         |                              |
|-------------------------|------------------------------|
| 1. F. S. Alsmiller      | 16. C. Zeigler               |
| 2. R. G. Alsmiller, Jr. | 17. EPMD Reports Office      |
| 3. B. R. Appleton       | 18-19. Laboratory Records    |
| 4. D. E. Bartine        | Department                   |
| 5. B. L. Bishop         | 20. Laboratory Records,      |
| 6-10. T. A. Gabriel     | ORNL-RC                      |
| 11. D. T. Ingersoll     | 21. Document Reference       |
| 12. J. K. Ingersoll     | Section                      |
| 13. R. A. Lillie        | 22. Central Research Library |
| 14. F. C. Maienschein   | 23. ORNL Patent Section      |
| 15. RSIC                |                              |

## EXTERNAL DISTRIBUTION

24. Office of Assistant Manager, for Energy Research and Development, Department of Energy, Oak Ridge Operations, P.O. Box 2001, Oak Ridge, TN 37831
- 25-34. Office of Scientific and Technical Information, P.O. Box 62, Oak Ridge, Tennessee 37830
35. Argonne National Laboratory, Library Services Dept., 302-CE125, 9700 S. Cass Avenue, Argonne, IL 60439
36. T. W. Armstrong, Science Applications, Inc., PO Box 2807, La Jolla, CA 92038
37. Miguel Awschalom, National Accelerator Laboratory, PO Box 500, Batavia, IL 60510
38. V. S. Barashenkov, Laboratory of Theoretical Physics, Joint Institute for Nuclear Research, Head Post Office, PO Box 79, Moscow, USSR
39. Gerald W. Bennett, Brookhaven National Laboratory, Upton, NY 11973
40. D. Berley, National Science Foundation, Washington, DC 20550
41. Elliott Bloom, Stanford Linear Accelerator Center, PO Box 4349, Stanford, CA 94305
42. J. Brau, University of Oregon, Eugene, OR 97403
43. Bruce Brown, Fermi National Accelerator Laboratory, PO Box 500, Batavia, IL 60510
44. David O. Caldwell, Dept. of Physics, University of California, at Santa Barbara, Santa Barbara, CA 93106
45. Stanley B. Curtis, Lawrence Radiation Laboratory, Bldg. 29, Room 213, Berkeley, CA 94720
46. Herbert DeStaebler, Stanford Linear Accelerator Center, Stanford University, Stanford, CA 94305
47. Tom Dombeck, Div. of High Energy & Nucl. Phys., ER-221, U.S. Department of Energy, 19901 Germantown Road, Germantown, Md 20874
48. A. DiCiaccio, CERN, Geneva 23, Switzerland
49. J. J. Dorning, Dept. of Nucl. Eng., and Engineering Physics, University of Virginia, Charlottesville, VA 22901

50. R. D. Edge, Physics Department, University of South Carolina, Columbia, SC 29208
51. R. Eisenstein, Department of Physics, University of Illinois, Urbana, IL 61801
52. R. W. Ellsworth, George Mason University, Fairfax, VA 22030
53. Chris Fabjan, CERN, Geneva 23, Switzerland
54. G. Feldman, Stanford Linear Accelerator Center, Stanford University, Stanford, CA 94305
55. W. T. Ford, Experiment 1A-Lab C, Fermi National Accelerator Laboratory, PO Box 500, Batavia, IL 60510
56. E. Fowler, Department of Physics, Purdue University, West Lafayette, IN 47907
57. H. T. Freudenreich, University of Maryland, College Park, MD 20742
58. E. Freytag, Deutsches Elektronen-Synchrotron, DESY, 2 Hamburg Drive, Flottbek, Notkesteig 1, West Germany
59. A. F. Garfinkel, Purue University, Dept. of Physics, W. Lafayette, IN 47907
60. M. G. D. Gilchriese, SSC Central Design Group, Lawrence Berkeley Laboratory, Berkeley, CA 94720
61. G. T. Gillies, Department of Physics, University of Virginia, Charlottesville, VA 22901
62. G. E. Gladding, University of Illinois, Department of Physics, Urbana, IL 61801
63. K. Goebel, Health Physics Group, CERN, 1211 Geneva 23, Switzerland
64. J. A. Goodman, University of Maryland, College Park, MD 20742
65. M. Goodman, Bell Communication Research, Morristown, NJ 07960
66. D. Groom, SSC Central Design Group, Lawrence Berkeley Laboratory, Berkeley, CA 94720
67. Herman Grunder, Deputy Director, General Sciences, Lawrence Berkeley Laboratory, 1 Cyclotron Rd, Berkeley, CA 94720
68. H. J. Hargis, University of Tennessee, Department of Physics, Knoxville, TN 37919
69. Frenc Hajnal, Health and Safety Laboratory, U.S. Department of Energy, 376 Hudson St, New York, NY 120014
70. R. M. Haralick, Department of Electrical Engineering, University of Washington, Seattle, WA 98195
71. M. Hofert, CERN, 1211 Geneva 23, Switzerland
72. Terrence Jensen, Department of Physics & Astronomy, The University of Rochester, Rochester, NY 14726
73. D. Lal, Tata Institute of Fundamental Research, National Centre of the Government of India, for Nuclear Science & Mathematics, Homi Bhabha Rd, Bombay 5, India
74. Lawrence Livermore Laboratory, Technical Information Department, PO Box 808, Livermore, CA 94550
75. V. Lebedev, Institute of High Energy Physics, Serpukhov, Moscow Region, USSR
76. Library for Nuclear Science, Massachusetts Institute of Technology, at Middleton, Middleton, MA 01949
77. J. LoSecco, Department of Physics, California Institute of Technology, Pasadena, CA 91125

78. J. Marks, Accelerator Fusion Research Division, Lawrence Berkeley Laboratory, 1 Cyclotron Rd, Berkeley, CA 94720
79. A. I. Mincer, University of Maryland, College Park, MD 20742
80. V. S. Narashimham, Tata Institute of Fundamental Research, Bombay 400 005, India
81. W. R. Nelson, Stanford Linear Accelerator Center, Stanford University, PO Box 4349, Stanford, CA 94305
82. T. R. Palfrey, Jr., Department of Physics, Purdue University, West Lafayette, IN 47907
83. Robert Palmer, Brookhaven National Laboratory, Upton, NY 11973
84. C. W. Peck, Department of Physics, California Institute of Technology, Pasadena, CA 91109
85. J. Ranft, Karl-Marx University, Physics Section, Linnestrasse 5,701, Leipzig, East Germany
86. Lincoln Read, Division of High Energy, and Nuclear Physics, Department of Energy, Washington, DC 20545
87. Jim Reidy, University of Mississippi, University, MS 38677
88. Enloe T. Ritter, Div. of High Energy & Nucl. Phys., ER-221, U.S. Department of Energy, 19901 Germantown Rd, Germantown, Md 20874
89. C. Rubbia, Lyman Laboratory, Harvard University, Cambridge, MA 02138
90. W. Schmidt, Institute of Experimental Nucl. Phys., University of Karlsruhe, 75 Karlsruhe, West Germany
91. The Secretary, Radiation Group, Lab II, CERN, 1211 Geneva 23, Switzerland
92. Walter Selove, University of Pennsylvania, Department of Physics, Philadelphia, PA 19104
93. B.S.P. Shen, Department of Astronomy, University of Pennsylvania, Philadelphia, PA 19104
94. M. Shupe, Department of Physics, University of Minnesota, Minneapolis, MN 55455
95. Alan Stevens, Physics Department, Brookhaven National Laboratory, Upton, NY 11973
96. G. R. Stevenson, Radiation Protection Group, Lab II, CERN, 1211 Geneva 23, Switzerland
97. L. Sulak, Department of Physics, University of Michigan, Ann Arbor, MI 48109
98. R. F. Taschek, Los Alamos National Laboratory, PO Box 1663, Los Alamos, NM 87544
99. R. Tesch, DESY, Hamburg, Notkesteig 1, West Germany
100. R. H. Thomas, Lawrence Radiation Laboratory, Health Physics Department, Bldg. 72, Berkeley, CA 94720
101. V. D. Toneev, Laboratory of Theoretical Physics, Joint Institute for Nuclear Research, Head Post Office, PO Box 79, Moscow, USSR
102. S. C. Tonwar, University of Maryland, College Park, Md 20742
103. W. Turchinets, Massachusetts Institute of Technology, R26-411, Cambridge, MA 02139
104. Jim Walker, University of Florida, Gainesville, FL 32611
105. W. J. Willis, CERN, Geneva 23, Switzerland
106. D. Winn, Lyman Laboratory, Harvard University, Cambridge, MA 02138
107. J. Wilczynski, Nuclear Research Center, Karlsruhe, West Germany

108. S. Yellin, Stanford University, Stanford Linear Accelerator Center, PO Box 4349, Stanford, CA 94305
109. G. B. Yodh, University of Maryland, College Park, Md 20742
110. S. Youssef, SCRI, Florida State University, Tallahassee, FL 32306
111. B. Zeitnitz, Nuclear Research Center, Karlsruhe, West Germany